34th Annual International Conference of the IEEE EMBS
San Diego, California USA, 28 August - 1 September, 2012

Implementation of Topographically Constrained Connectivity for a Large-Scale Biologically Realistic Model of the Hippocampus

Gene J. Yu, *Student Member*, *IEEE*, Brian S. Robinson, *Student Member*, *IEEE*, Phillip J. Hendrickson, *Member*, *IEEE*, Dong Song, *Member*, *IEEE*, and Theodore W. Berger, *Fellow, IEEE*

Abstract — **In order to understand how memory works in the brain, the hippocampus is highly studied because of its role in the encoding of long-term memories. We have identified four characteristics that would contribute to the encoding process: the morphology of the neurons, their biophysics, synaptic plasticity, and the topography connecting the input to and the neurons within the hippocampus. To investigate how long-term memory is encoded, we are constructing a large-scale biologically realistic model of the rat hippocampus. This work focuses on how topography contributes to the output of the hippocampus. Generally, the brain is structured with topography such that the synaptic connections formed by an input neuron population are organized spatially across the receiving population. The first step in our model was to construct how entorhinal cortex inputs connect to the dentate gyrus of the hippocampus. We have derived realistic constraints from topographical data to connect the two cell populations. The details on how these constraints were applied are presented. We demonstrate that the spatial connectivity has a major impact on the output of the simulation, and the results emphasize the importance of carefully defining spatial connectivity in neural network models of the brain in order to generate relevant spatiotemporal patterns.**

I. Introduction

Biological memory is one of the most sought-after constructs in the world, yet still, its mechanisms of action remain elusive. The hippocampus has been identified as one of the key structures involved with the encoding of short-term memories into long-term memories, but the nature of its encoding process and how it performs this encoding process is not yet understood. To gain insight into biological memory, not only is it important to characterize what the encoding is (i.e. the input-output characteristics of the hippocampus), it is important to understand the properties of the hippocampus that allow such encoding to be performed.

We have identified four major characteristics that contribute to the input-output behavior of the hippocampus: the morphology of the neurons, their biophysics, non-stationary behavior (i.e. synaptic plasticity), and topography. Not only are the individual characteristics important, the interaction among these components further affect the output of the hippocampus.

Large-scale, biologically realistic modeling can provide a means to quantify and systematically interrogate the hippocampus. Using parametric modeling, these four characteristics can be explicitly modeled, and their combined effects can be explored. A general framework addressing these themes for creating a large-scale biologically realistic model of the rat hippocampus has been proposed by Hendrickson *et. al.* in these proceedings [2]. The implementation of synaptic plasticity is detailed by Robinson *et. al.* also in these proceedings [3]. Here, the impact of topography is explored. This work presents the approach for implementing anatomically based spatial connectivity for a large-scale, biologically realistic model of the rat hippocampus. Specifically, the topography governing the connectivity between the entorhinal cortex (EC) and the dentate gyrus (DG) is defined and applied.

The trisynaptic pathway is the main information processing pathway in the hippocampus, and it can be summarized as follows: Perforant path input from the EC is received by the DG of the hippocampus. The dentate gyrus projects onto the CA3 pyramidal cells, and CA3 projects onto the CA1 pyramidal cells. CA1 provides the output of the hippocampus [1].

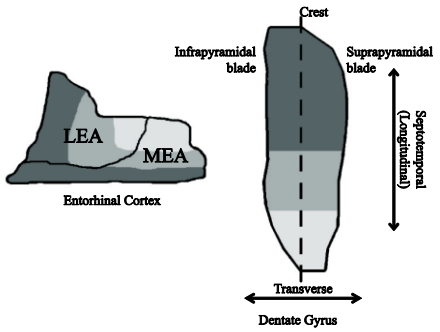

Figure 1. Summary of the bands presented by Dolorfo and Amaral. Cells from the bands in the EC map to the corresponding colored areas on the DG. The 2-D postsynaptic absolute map of the DG is depicted.

Experimental data shows that the input to the DG is distributed in a structured manner [4]. This structure must be significant because brain is seldom organized without intent. The mapping of the EC axons onto the dentate gyrus has been described as three discrete bands on the EC which map to three regions along the septotemporal length of the DG (Fig. 1) [4]. These bands were identified by Dolorfo and Amaral by injecting retrograde tracers systematically down the length of rat dentate gyri and identifying the corresponding labeled areas on the EC. Using this data, the locations of the perforation points could be constrained to a region on the DG given the spatial location of the EC cells. Although the paper concludes that there are three discrete bands in the EC which project to three areas in the DG, we

G. J. Yu, B. S. Robinson, P. J. Hendrickson, D. Song and T. W. Berger are with the Center for Neural Engineering, Department of Biomedical Engineering, University of Southern California, Los Angeles, CA 90089 USA (e-mail: geneyu@usc.edu; bsrobins@usc.edu; phendric@usc.edu; dsong@usc.edu; berger@bmsr.usc.edu)

have reinterpreted the data to create four bands which also overlap over each other.

The iteration of the EC to DG model used to test the application of topography contains three cell types: lateral entorhinal area (LEA) cells, medial entorhinal area (MEA) cells, and DG granule cells. Layer II LEA and MEA cells synapse with the granule cells on the outer third and middle third of the dendritic tree, respectively [5]. A map for the presynaptic (EC) and postsynaptic (DG) populations were created called the presynaptic and postsynaptic absolute map. Upon these maps, the cell populations could be seeded, and the connectivity matrix could be applied. These maps are useful because spatially dependent characteristics of the neurons could also be varied. However, these variations were not explored in this paper. Connecting a presynaptic neuron to a postsynaptic neuron required the following conditions to be met: the presynaptic axon must be in physical contact with postsynaptic dendritic tree, and a dendritic spine must be available with which to form a synapse. Thus, the presynaptic axon terminal field, the postsynaptic dendritic tree spread, and the number of spines on the postsynaptic cells needed to be defined. Two different connectivity schemes are presented to demonstrate the impact of spatial connectivity: a random EC to DG connectivity and a topographically constrained connectivity.

II. Methods

A. Defining the Postsynaptic Absolute Map and Seeding the Granule Cells

The postsynaptic absolute map was based on the geometry of the rat dentate gyrus. The DG structure is comparable to a rectangle sheet that has been folded in the middle down its length to form a "C"-shape. The fold is known as the crest, and it divides the sheet into the infrapyramidal and suprapyramidal blades. In reality, the width of the rectangle is not constant along its length. Therefore, the postsynaptic absolute map was approximated using a series of trapezoids using the widths that were measured along its septotemporal length with a total length of 10 mm (Fig. 1) [6]. The postsynaptic absolute map axes were defined to be the distance along the curvature from the crest, so the map could be represented in 2-D (Fig. 1). The distribution of cell density in the dentate gyrus was identified and used to seed the granule cell population onto the absolute map. Each soma corresponded to an x- and y-coordinate on the postsynaptic absolute map.

B. Creating the EC to DG Connectivity Matrix

The plots published by Dolorfo and Amaral were digitized, and the EC plots that mapped to the same DG quartile were averaged in order to measure the mean percentage of the EC that each band covered. Thus, assuming a uniform density of cells throughout the EC, the number of cells associated with each band could be calculated by multiplying the total number of cells by the percentage of the MEA or LEA covered by each band. In this manner, the presynaptic absolute map was collapsed into two 1-D arrays that contained all of the cells in each EC sub-section and organized by the bands. One array contained the MEA cells, and the other contained the LEA cells. Four bands were identified, and each band on the EC targeted a specific quartile along the septotemporal length on the dentate gyrus. Each quartile corresponded to 25% of the septotemporal length of the dentate gyrus, organized sequentially from the top of the dentate gyrus to the bottom. If any overlap occurred between bands on the EC, then the cells that fell in the overlap targeted both of the quartiles that contributed to the overlap. The target quartiles correspond to the region where the perforation point of an EC cell can be placed on the postsynaptic absolute map (Fig. 2). For the EC cells that map to a certain quartile or quartiles, their perforation points were given a uniform random distribution within that region.

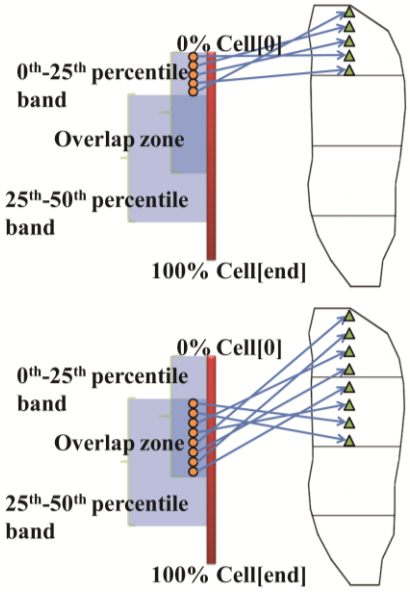

Figure 2. Symbolic representation of the spatial connectivity mapping EC cells (left) to the DG (right) with a uniform random distribution. The absolute map of the EC is reduced to a 1-D array and is represented by the red bar with the first cell at the top and the last cell at the bottom. The lengths of the blue boxes symbolize the proportion of cells that map to a certain quartile. Overlap occurs in the darker blue boxes, and those cells can map to either quartile that contributes to the band (bottom). The sizes of the boxes do not represent the actual percentages used by the model and are for demonstrative purposes.

C. Defining the Presynaptic Axon Terminal Field

The axon terminal field of the perforant path has been shown to conform to the curvature of the dentate gyrus, and because the postsynaptic absolute map represents a flat surface, the shape of the axon terminal field given a 2-D representation. Because there was little information characterizing the actual shape of the field, the shape was approximated to be a rectangle. The axon terminal field of the cell was centered on its perforation point, and the field was defined to cover the entire transverse of the dentate gyrus with a longitudinal length that was randomly and uniformly chosen to be between 1.0 and 1.5 mm [7]. MEA cells and LEA cells were given the same terminal field constraints.

D. Defining the Postsynaptic Dendritic Tree

On the postsynaptic absolute map, the granule cell dendrite tree was approximated to be a point. Due to the axon terminal field covering the entire transverse extent of the dentate gyrus, the transverse spread of the dendritic tree was not considered [7]. The mean longitudinal spread of 171 μm was also considered negligible compared to the axon terminal field's longitudinal spread of 1.0 to 1.5 mm [8].

E. Connecting the Populations

For each granule cell, we created a list of all the EC cells whose axon terminal fields overlapped with that granule cell's location. This list contained all of the possible presynaptic candidates. Presynaptic cells were randomly chosen until the available spine pool was depleted. MEA cells could only connect to spines in the middle third of the dendrite tree, and LEA cells were limited to the outer third. A check would be made to ensure that the same presynaptic cell did not connect to the same postsynaptic cell more than 3 times. The change in conductance due to the activation of the synapses was modeled as a double exponential with time constants of 1.05 ms and 5.75 ms.

F. Granule Cell Model

Compartmental models of the granule cells were created in NEURON v7.2. Unique morphologies were generated for each cell resulting in complex, branching dendrites. The ion channels added to each cell include a sodium channel, various potassium channels, calcium dependent potassium channels, and calcium channels. For more detailed information on the generation of the morphology and the conductances and distribution of the ion channels, refer to Hendrickson *et. al.* from these proceedings [2].

G. Observing the Effect of Topography

Two networks were constructed using NEURON v7.2 with a simulated time of 1500 ms, a topographically constrained network and a random network. In the topographically constrained network, the EC cells with which a granule cell could connect were limited to a subset of the EC cell population determined by the topography. In the random network, every EC cell was available to synapse with any DG cell following a uniform random distribution. Whenever it was necessary, pseudo random numbers were generated to make the simulations repeatable. Both simulations were scaled down to $1/10^{th}$ of the actual number of cells to test this initial implementation of the model**:** 100,000 granule cells, 1,000 basket cells, 6,600 MEA cells, and 4,600 LEA cells [5], [9]. The MEA cells were assigned a random inter-spike interval defined by a Poisson distribution and a randomly chosen mean between 1.5 and 3.5 Hz while the LEA cells had a randomly chosen mean firing rate between 3.5 and 8.0 Hz. Both networks used the same input patterns meaning that an EC cell with a given ID would generate the same input pattern. The key difference lay in the connectivity scheme which would cause the input pattern to innervate different regions of the DG.

III. Results

A. Validation of the Bands

Before investigating the impact of the connectivity schemes, a series of tests were run that activated only the cells that belonged to a particular band or overlap region (Fig. 3). The EC cells were given a mean Poisson firing rate of 25 Hz, and 50 ms of granule cell activity was simulated. The locations of action potentials were collected across the simulation time and plotted on the postsynaptic absolute map. Thus, we were able to demonstrate that the locations of the perforation points of the EC subgroups were properly constrained to their assigned quartiles.

B. Topographically Constrained vs. Random Connectivity

Under inputs of Poisson noise, the random network resulted in an output almost resembling Poisson noise (Fig. 4). However, there are definite stripes of activity showing spatially and temporally synchronous firing along the septotemporal axis of the dentate gyrus. Using the same input patterns as the random network, the topographically constrained network resulted in an asynchronous output with varying spatiotemporal patterns (Fig. 4). Not only are local regions of high density activity are seen, but no two regions of spatial activity are alike. Each cluster of activity has a different center position, height, and width. These characteristics signify the septotemporal level at which the

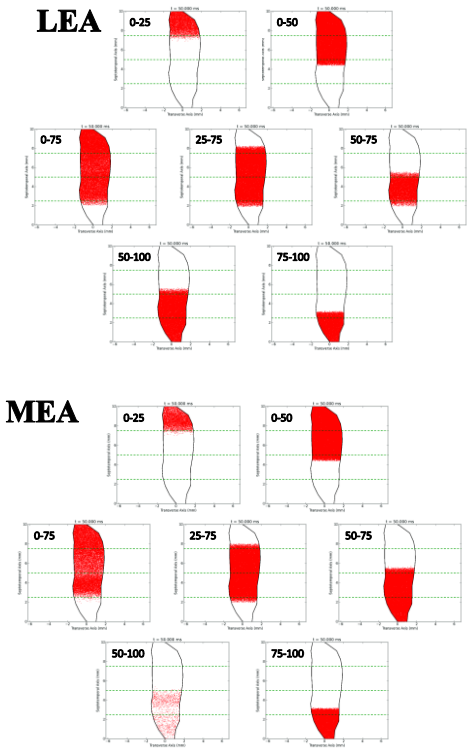

Figure 3. Validation of the connectivity matrix implementation. The subsets of cells that belonged to a particular band or overlap region in the EC were activated. The red dots signify the location of the granule cells that fired an action potential over 50 ms. Activity beyond the quartiles can be seen only the perforation points, not the axon terminal fields were constrained by the quartiles.

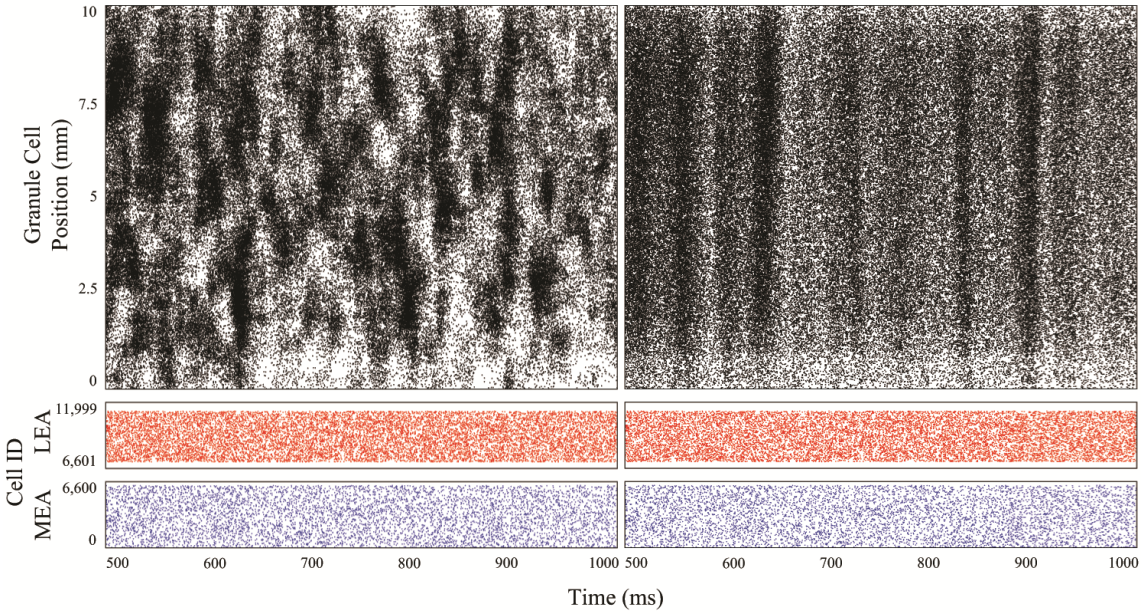

Figure 4. Output of the networks using the topographically constrained connectivity (left) and using random connectivity (right). Each point represents an action potential being fired at that time. The MEA and LEA cells are plotted by their cell ID, and the granule cells are plotted versus based on their septotemporal position on the DG. Only 500 ms of the simulation are shown in order to keep the plots from being too dense.

increased activity is centered, the spatial extent of the increased activity, and the duration in time of increased activity, respectively, and they highlight the variability of the spatiotemporal pattern.

IV. Discussion

The results of the simulations show that the connectivity scheme implemented in a network significantly impacts the spatiotemporal output pattern of the model. Without commenting on the how realistic the patterns of the network are, the differences between the outputs of the networks demonstrate how the topography of connections need to be carefully considered when attempting to generate realistic spatiotemporal patterns in neuron network models.

Although the visual differences between these plots are apparent, as the complexity of the large-scale model and its spatiotemporal patterns increase, the current visualizations will not be sufficient in describing the characteristics of the raster plots. This motivates a need to present or analyze the data in a different way such that the important features can be more intuitively observed. Metrics that can quantify aspects of the raster plots would also be useful to convey the differences between plots in a more objective and quantitative manner.

Using the current methodological approach, the subsequent areas of the trisynaptic pathway will be incorporated into the large-scale model while preserving the spatial connectivity between the populations.

Acknowledgment

Computation for the work described in this paper was supported by the University of Southern California Center for High-Performance Computing and Communications (www.usc.edu/hpcc).

References

[1] P. Andersen, T.V.P. Bliss, and K. K. Skrede. "Lamellar Organization of Hippocampal Excitatory Pathways," *Experimental Brain Research*, vol 13, pp. 222–238, 1971.

[2] P. J. Hendrickson, G.J. Yu, B. S. Robinson, D. Song, and T. W. Berger, "Toward a Large-Scale Biologically Realistic Model of the Hippocampus," *34th Annual International Conference of the IEEE EMBS*, 2012.

[3] B. Robinson, G. Yu, P. Hendrickson, D. Song, and T. Berger. "Implementation of Activity-Dependent Synaptic Plasticity Rules for a Large-Scale Biologically Realistic Model of the Hippocampus," *34th Annual International Conference of the IEEE EMBS*, 2012.

[4] C. L. Dolorfo and D. G. Amaral, "Entorhinal cortex of the rat: topographic organization of the cells of origin of the perforant path projection to the dentate gyrus," *The Journal of Comparative Neurology*, vol. 398, no. 1, pp. 25-48, Aug. 1998.

[5] D. G. Amaral, H. E. Scharfman, and P. Lavenex, "The dentate gyrus: fundamental neuroanatomical organization (dentate gyrus for dummies)," *Progress in brain research*, vol. 163, pp. 3-22, Jan. 2007.

[6] F. B. Gaarskjaer, "Organization of the mossy fiber system of the rat studied in extended hippocampi. I. Terminal area related to number of granule and pyramidal cells," *The Journal of comparative neurology*, vol. 178, no. 1, pp. 49-72, Mar. 1978.

[7] N. Tamamaki and Y. Nojyo, "Projection of the entorhinal layer II neurons in the rat as revealed by intracellular pressure-injection of neurobiotin," *Hippocampus*, vol. 3, no. 4, pp. 471-80, Oct. 1993.

[8] B. J. Claiborne, D. G. Amaral, and W. M. Cowan, "Quantitative, three-dimensional analysis of granule cell dendrites in the rat dentate gyrus," *The Journal of comparative neurology*, vol. 302, no. 2, pp. 206-219, Dec. 1990.

[9] W. H. Mulders, M. J. West, and L. Slomianka, "Neuron numbers in the presubiculum, parasubiculum, and entorhinal area of the rat," *The Journal of comparative neurology*, vol. 385, no. 1, pp. 83-94, Aug. 1997.